Ocean regulation hypothesis for glacier dynamics in southeast Greenland and implications for ice sheet mass changes

T. Murray,[1] K. Scharrer,[1] T. D. James,[1] S. R. Dye,[2] E. Hanna,[3] A. D. Booth,[1] N. Selmes,[1] A. Luckman,[1] A. L. C. Hughes,[1] S. Cook,[1] and P. Huybrechts[4]

Received 9 September 2009; revised 31 March 2010; accepted 5 April 2010; published 19 August 2010.

[1] Synchronous acceleration and thinning of southeast (SE) Greenland glaciers during the early 2000s was the main contributor that resulted in the doubling of annual discharge from the ice sheet. We show that this acceleration was followed by a synchronized and widespread slowdown of the same glaciers, in many cases associated with a decrease in thinning rates, and we propose that ice sheet–ocean interactions are the first-order regional control on these recent mass changes. Sea surface temperature and mooring data show that the preceding dynamic thinning coincides with a brief decline in the cold East Greenland Coastal Current (EGCC) and East Greenland Current. We suggest this decline was partly induced by a reduction in ice sheet runoff, which allowed warm water from the Irminger Current to reach the SE Greenland coast. A restrengthening of the cold waters coincides with the glaciers' subsequent slowdown. We argue that this warming and subsequent cooling of the coastal waters was the cause of the glaciers' dynamic changes. We further suggest that the restrengthening of the EGCC resulted in part from cold water input by increased glacier calving during the speedup and increased ice sheet runoff. We hypothesize that the main mechanism for ice sheet mass loss in SE Greenland is highly sensitive to ocean conditions and is likely subject to negative feedback mechanisms.

Citation: Murray, T., et al. (2010), Ocean regulation hypothesis for glacier dynamics in southeast Greenland and implications for ice sheet mass changes, *J. Geophys. Res.*, *115*, F03026, doi:10.1029/2009JF001522.

1. Introduction

[2] During the early 2000s, the Greenland Ice Sheet's annual ice discharge doubled, primarily as the result of widespread glacier acceleration and consequent thinning of the ice sheet's southeast (SE) sector [*Luthcke et al.*, 2006; *Rignot and Kanagaratnam*, 2006; *Howat et al.*, 2008; *Wouters et al.*, 2008]. During the period 2003–2005, southeast (SE) Greenland's outlet glaciers were dramatically thinning [*Stearns and Hamilton*, 2007; *Howat et al.*, 2007, 2008], accelerating [*Luckman et al.*, 2006; *Rignot and Kanagaratnam*, 2006; *Howat et al.*, 2008], and retreating [*Howat et al.*, 2007, 2008; *Moon and Joughin*, 2008]. Then, during 2006, two of the largest outlet glaciers in the sector, Helheim and Kangerdlugssuaq, were reported to have slowed down simultaneously [*Howat et al.*, 2007], ceased thinning [*Stearns and Hamilton*, 2007; *Howat et al.*, 2007], and readvanced [*Joughin et al.*, 2008], and there was some indication that other glaciers in the region followed suit [*Howat et al.*, 2008; *Moon and Joughin*, 2008]. Insufficient understanding of the controls on the speed of these outlet glaciers meant it was unknown whether these changes represented profound alterations in the ice sheet mass budget or simply a short-lived event. Furthermore, it was unclear whether the slowdown was regionally widespread and synchronous, or whether individual glaciers were responding to local factors, for example, fjord bathymetry as suggested by both *Howat et al.* [2008] and *Nick et al.* [2009].

[3] The synchronous nature of the speedup event suggests a regional forcing [e.g., *Luckman et al.*, 2006]. Two possible regional forcings that can affect tidewater glaciers are atmospheric and fjord/ocean temperatures.

[4] Atmospheric warming can cause increased surface meltwater and, if this water reaches the glacier bed, affect glacier speeds by increasing lubrication and hence basal sliding. This is a well-known effect for valley glaciers and was first reported to occur on the Greenland Ice Sheet by *Zwally et al.* [2002]. Additional meltwater feeding into crevasses close to the glacier margin may also result in higher calving rates [*Benn et al.*, 2007]. Also fresh and buoyant subglacial water originally derived from surface melt that is released at the front margin can drive convection of warm fjord water and greatly increase calving cliff melt rates [*Motyka et al.*, 2003], causing undercutting and enhanced calving rates.

[1]GLIMPSE Research Group, Department of Geography, Swansea University, Swansea, UK.
[2]Centre for Environment Fisheries and Aquaculture Science, Lowestoft Laboratory, Lowestoft, UK.
[3]Department of Geography, University of Sheffield, Sheffield, UK.
[4]Department of Geography, Vrije Universiteit Brussel, Brussels, Belgium.

0148-0227/10/2009JF001522

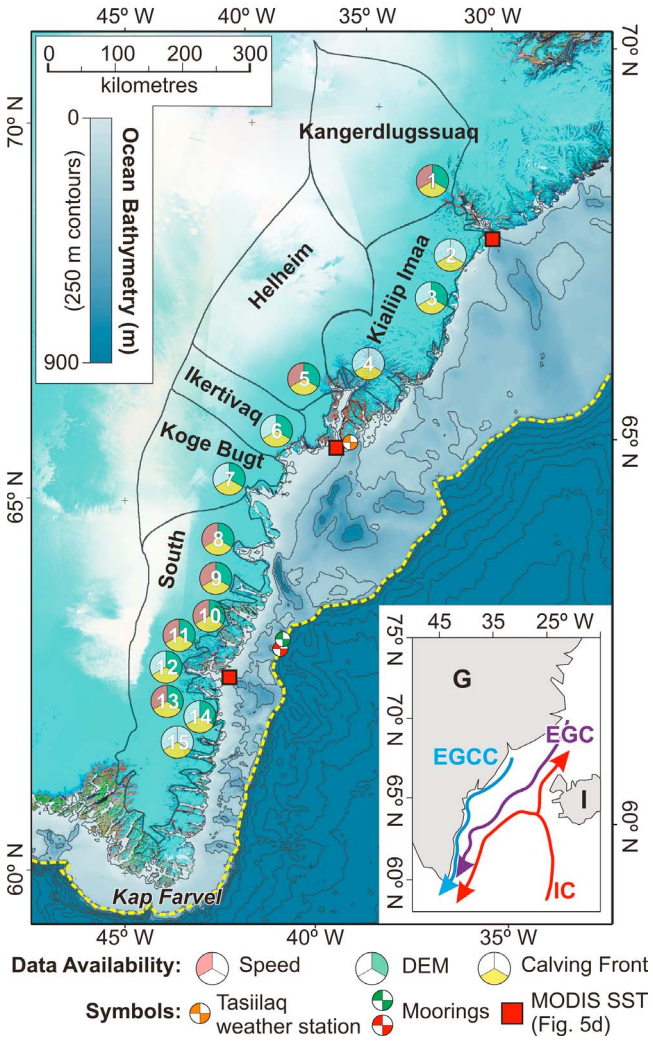

Figure 1. SE Greenland location map. The figure is a composite of Landsat Zulu images (https://zulu.ssc.nasa.gov/mrsid/) and IBCAO bathymetry data [*Jakobsson et al.*, 2008] (see http://www.ibcao.org). Bathymetric contours at 250 m depth intervals, yellow dashed lines shows the shelf break. While bathymetric data are indicative, there are likely to be limitations, especially close to the shore as this region is unfrequented by shipping. Labels 1–15 denote major outlet glaciers: 1, Kangerdlugssuaq; 2, Nordre; 3, Kruuse; 4, Midgard; 5, Helheim; 6, Ikertivaq; 7, Koge Bugt; 8, Gyldenlove; 9, Bernstorff; 10, Skinfaxe, Guldfaxe and Rimfaxe; 11, Heimdal; 12, Tingmiarmiut; 13, Mogens; 14, Puistortuq; 15, Takissoq. Some glaciers comprise several outlets under a single name. Bold face text refers to catchment names delineated by black lines. Inset: after *Sutherland* [2008]. IC, Irminger Current; EGC, East Greenland Current; EGCC, East Greenland Coastal Current; G, Greenland; I, Iceland.

[5] Warm surface water in the fjords can reduce the duration and extent of fjord ice as well as the presence and integrity of the ice mélange that forms in front of many of these SE Greenland tidewater glaciers. The mélange consists of small pieces of calved ice and sea ice (we have used the term mélange in preference to "sikkusak" to maintain consistency with *Amundson et al.* [2010]). Reduction in fjord ice will significantly lower the albedo and thus increase atmospheric warming, as well as increasing the length of time when the glacier's front margin is exposed to wave action. The presence of an ice mélange may provide backstress to the glacier, stabilizing the calving front [*Amundson et al.*, 2010], as well as potentially changing circulation within the fjord [c.f., *Motyka et al.*, 2003]. Warm water can also increase undercutting of the glacier's highly sensitive calving front [*Motyka et al.*, 2003; *Nick et al.*, 2009] and, if the front is floating, greatly increase basal melt rates [*P. R. Holland et al.*, 2008]. Furthermore, thinning of the glacier tongue can cause reduced effective pressures beneath the glacier, promoting faster flow [*Pfeffer*, 2007].

[6] In this paper, we describe the oceanographic setting of the SE Greenland region and then undertake two analyses to explore the relationship between oceanic processes and glacier dynamics. First, we report flow speeds, surface elevation, and calving front positions for a large number of tidewater terminating glaciers in SE Greenland. These data build on and add detail to the analysis reported in the work of *Howat et al.* [2008]. We focus on the regions of highest mass loss [*Luthcke et al.*, 2006; *Wouters et al.*, 2008] and the time period 2004–2008, following the speedup event. Our data show that the slowdown from 2006 was widespread and synchronized throughout SE Greenland, and except a minor reactivation at Helheim during 2007, continued until at least 2008. Second, we explore the possible causes of this speedup and subsequent slowdown. We show the glacier speedup between 2003 and 2005 was not driven by increases in the amount of surface meltwater but coincided with the presence of warm water, probably of Irminger Current origin, at the coast; furthermore, the period of fast flow ended when cold water returned to the coast. We present evidence that that the speedup was probably terminated in part by increased discharge from the glaciers themselves, which increased ice sheet runoff and iceberg calving. This discharge introduced additional cold water strengthening the East Greenland Coastal Current (EGCC). Finally, we argue that this negative feedback of ice sheet–derived cold water strengthening the coastal current helped prevent continued very fast mass loss from the Greenland Ice Sheet.

2. Oceanographic Setting

[7] The continental shelf in the SE Greenland region varies from 60 to 200 km wide and is typically a few hundreds of meters deep (Figure 1). Deep troughs are eroded into the shelf extending from the fjords of all the current major outlet glaciers. For example, the trough of Kangerdlugssuaq glacier is more than 500 m deep and ~300 km long, and those of Helheim and Glydenlove glaciers are more than 750 m deep and ~250 and ~100 km long, respectively. In contrast with west Greenland fjords, the literature suggests these SE Greenland fjord/trough systems do not have sills [*Buch*, 2002]. The IBCAO bathymetry data [*Jakobsson et al.*, 2008] (see http://www.ibcao.org) shows the troughs shallowing toward the shelf edge, with depths ~350–400 m at the shelf-break, and also shallowing toward the coast (Figure 1). These data are more robust in regions frequented by shipping, so the former is likely to be correct, but the data are especially unlikely to be robust near the SE Greenland coast. For example where shallow water (~200 m) is shown at the mouth

of Helheim Glacier's Sermilik Fjord, our measurements show depths of ~900 m.

[8] Figure 1 shows ocean circulation patterns along the SE Greenland coast. The warm Irminger Current (IC) transports high-salinity water northward from the Atlantic. The current bifurcates to the west of Iceland, and one branch flows southward along the SE Greenland coast. Situated between the IC and the coast are the cold East Greenland Current (EGC), which transports low salinity water of Arctic origin southward, and the East Greenland Coastal Current (EGCC). The EGCC flows southward along the coast on the landward side of the continental shelf [*Bacon et al.*, 2002] (Figure 1) and is composed of fresh, cold water [*Bacon et al.*, 2002; *Sutherland et al.*, 2009]. The current is ~15 km wide, ~100 m deep and has peak surface speeds of ~0.5–1 m s^{-1} [*Bacon et al.*, 2002; *Sutherland and Pickart*, 2008]. The EGCC has been suggested to be an inshore branch of the cold East Greenland Current, routed to the coast through major glacial troughs [*Sutherland and Pickart*, 2008]. Profiles of temperature, salinity, and flow velocity across the continental shelf show that the EGCC starts at Kangerdlugssuaq is strongest at the latitude of Helheim Glacier and weakens further south (Figure 1) [*Sutherland et al.*, 2009].

[9] Observations suggest that a component of the EGCC originates from the ice sheet [e.g., *Bacon et al.*, 2002], with water input from the SE Greenland coast, particularly during summer; however, there is debate concerning the relative contribution to the EGCC of ice sheet versus sea ice sources [*Bacon et al.*, 2002; *Sutherland et al.*, 2009]. Water salinity and temperature increase with distance offshore and from the surface toward the bottom at Kap Farvel (location in Figure 1), which supports the assertion that a freshwater component originates from onshore [*Bacon et al.*, 2002]. Moreover, sea ice export through the Fram Strait typically ceases during July/August [*Sandven et al.*, 2007]. *Sutherland and Pickart* [2008] showed that the melt of sea ice sourced primarily from the Fram Strait, meltwater from the Greenland Ice Sheet (via calved ice and runoff), and other Arctic freshwater sources contributed ~10–12% volumetrically to the EGCC during 2004. The analyses in our paper provide further evidence that the relative contribution to the EGCC of sea ice melt and ice sheet runoff vary through the summer months and between years, and we show that sea surface temperature data evidence warm water diverted to the coast during the summer along the Kangerdlugssuaq trough.

3. Methods

3.1. Measurement of Glacier Flow Speed, Surface Topography, and Terminus Positions

[10] We derived flow speeds of nine major tidewater outlets from the SE Greenland Ice Sheet (Figure 1) using cross-correlation feature tracking [*Scambos et al.*, 1992; *Strozzi et al.*, 2002] on pairs of ASTER, Landsat-7, and ENVISAT-ASAR images, and repeated lidar swaths. We choose summer images to derive speeds and are primarily interested in the interannual variations: seasonal speed variations of tidewater glaciers have been shown to be up to ~15% [*Joughin et al.*, 2008], so only changes larger than this should be considered significant. Glacier elevation changes were measured for 24 tidewater outlets by combining digital elevation models (DEMs) from ASTER satellite stereo images, extracted using PCI Geomatics Orthoengine, with airborne lidar and SPOT-5 DEMs. All DEMs were derived for summer (typically July–August) to minimize seasonal effects and allow us to elucidate long-term trends. Systematic errors between DEM pairs were reduced by matching elevations of stable rock areas. Even so, the accuracy of the DEMs from which these elevation changes were produced is considered to be ±10 m (ASTER and SPOT-5) and ±0.10 m (lidar). Changes in surface elevation were averaged along profiles, typically 10 km in length, but in some cases somewhat shorter (details are given with the results). The profiles extended upglacier from the furthest retreated calving front position and each had the same length during all epochs. Calving front positions, which can have intra-annual variations of several kilometers, were extracted for 36 glacier fronts from orthorectified imagery of the same sources. Our measurements of frontal positions used multiple images through the summer months (typically April–October).

3.2. Surface Mass Balance, Accumulation, and Runoff

[11] We estimated surface mass balance for each SE Greenland catchment (Figure 1) by extracting results from monthly modeled Greenland runoff and accumulation maps. The method for delineating catchment regions is based on a DEM and ice thickness data set [*Bamber et al.*, 2001]. Helheim and Kangerdlugssuaq's catchments are around 85% of the area of the south catchment (Figure 1), which is the largest in the region (Table 1).

[12] Runoff was modeled for the catchments using a degree-day model with different degree-day factors for snow and ice, taking into account surface meltwater retention by pore infilling and refreezing [*Hanna et al.*, 2005]. The model uses downscaled air temperatures from the European Center for Medium-Range Weather Forecasting (ECMWF), corrected for surface orography [*Ekholm*, 1996] and empirically derived lapse rates. The accumulation was modeled from ECMWF reanalyses. Both runoff and accumulation were calculated on a 5 km grid. Model errors were estimated to be 10% for runoff [*Hanna et al.*, 2005] and 20% for accumulation [*Hanna et al.*, 2006]. We also analyzed air-temperature data from Tasiilaq, which is at the coast and situated close to the Helheim and Ikertivaq catchments [*Cappelen et al.*, 2008].

3.3. Measurement of Ocean Temperature and Salinity

[13] Temperature and salinity were measured at hourly or higher temporal resolution at two moorings situated on the continental shelf (Figure 1) from summer 2000 to 2007. The first was an upper water column mooring at nominal depths of 20, 60, and 100 m, and the second was a seabed lander at ~220 m depth. Unfortunately, deployments of the upper mooring since summer 2004 have been unrecoverable, probably due to iceberg damage, while the lander was only in place after summer 2004.

3.4. Sea Surface Temperature

[14] Our mooring measurements provide high temporal resolution information about water column temperature and salinity, but only for a single profile. To investigate spatial variation in ocean conditions we produced a time series of mean sea surface temperature anomaly (SSTA) maps from advanced very high resolution radiometer (AVHRR) data and

Table 1. Catchment Characteristics and Results of Surface Mass Balance Model[a]

Catchment	Area (km^2)	Runoff 2003 (km^3)	October–April Accumulation 2002–2003 (km^3)	Runoff as % of Accumulation 2002–2003	Runoff 2007 (km^3)	October–April Accumulation 2006–2007 (km^3)	Runoff as % of Accumulation 2006–2007
Kanger	51,259	0.57	22.9	2.5	3.4	13.3	25
Kialiip Imaa	37,482	0.73	42.0	1.7	3.0	21.1	14
Helheim	51,856	0.43	30.9	1.3	1.6	19.2	8.4
Ikertivaq	15,557	0.00	21.7	0	0.49	13.0	13.8
Koge Bugt	27,008	0.00	37.1	0	0.76	18.6	4.1
South	60,332	8.78	89.0	9.9	21.8	42.0	52
Total	243,494	10.5	244	4	31.0	127	24

[a]For example, low (2003) and high (2007) runoff years. See Figure 1 for catchment locations and Figure 3 for the full data series.

used the same data to quantify SSTA along a profile located 1 pixel (the data have a resolution of 1°) from the coastline [*Reynolds et al.*, 2002; http://iridl.ldeo.columbia.edu/SOURCES/.NOAA/.NCEP/.EMC/.CMB/.GLOBAL/.Reyn_SmithOIv2/.monthly/.ssta/]. The Reynolds SST series uses the time period 1971–2000 as its baseline from which SSTAs are calculated. To allow higher resolution structure in the sea surface temperature (SST) to be identified, we also used a 4 km resolution weekly MODIS (Moderate Resolution Imaging Spectroradiometer) SST product [*Armstrong*, 2002] and the 60 m resolution thermal band (6.2 high gain) of Landsat-7 imagery. The Landsat data were converted to radiance using standard equations and the brightness temperature was calculated using the inverse Planck function (available at http://landsathandbook.gsfc.nasa.gov/handbook/handbook_htmls/chapter11/chapter11.html). Cloud and land were masked by applying a threshold in band 5, and the images dating from post-2003 were interpolated for presentation purposes to remove the striping resulting from the failure of the scanline correction. Finally, the brightness temperature was converted to SST by applying a +1°C correction following a statistical analysis of the Landsat brightness temperature values with temporally and spatially coincident calibrated MODIS data [*Armstrong*, 2002]. After this correction, 80% of the Landsat pixel values lie within ±0.7°C of the MODIS values, themselves considered to have an accuracy of ±0.25°C [*Armstrong*, 2002]. Finally, we mapped monthly sea ice coverage along the same coastal profile used for SSTA from the AVHRR sea ice product (http://iridl.ldeo.columbia.edu/SOURCES/.NOAA/.NCDC/.OISST/.version1/.AVHRR/.ice/).

4. Results

4.1. Glacier Flow Speed and Surface Topography

[15] Flow speeds for the glaciers studied were fastest during 2004 or 2005 (Table 2) (we do not have sufficient speed data to distinguish between 2004 and 2005 as the regionally fastest flow speed); subsequent to 2005, all glaciers slowed. There is evidence of a minor speedup during 2007 at Helheim, but by 2008 several glaciers were flowing at speeds close to or even slower than in 2000–2001 (Table 2 and Figure 2). The flow speeds of both Helheim and Kangerdlugssuaq glaciers doubled between 2001 and 2005. However, despite subsequently slowing, both remained at elevated flow speeds into 2008, at ~40% and ~60% above their 2001 flow speed, respectively.

[16] As the flow speed of these SE Greenland glaciers slowed after 2005, thinning measured along profiles from the front margin also slowed or ceased (Table 3). Mean glacier thinning rates were, on average, 10 times lower in 2005–2006 than 2004/2005, with median rates also showing the drop in thinning. Following this, in 2006–2007, the thinning rate dropped further (mean thinning rate 0.3 m a^{-1}, while the median value shows thickening at a rate of 1 m a^{-1}). Thinning resumed during 2007–2008 (mean value 4.2 m a^{-1}, median 3 m a^{-1}), but remained below the values of 2004–2005 (Table 3). While the actual values depend on the length of

Table 2. Speeds for Glacier Outlets[a]

Glacier Name[b]	Distance From 2008 Front (km)	Speed (m/d)						
		2000	2001	2004	2005	2006	2007	2008
Kanger	2.4		15.2 (L)	20.2 (E)	**35.7 (A)**	31.9 (A)	25.4 (D)	24.0 (E)
Helheim	4.9		15.0 (L)	22.9 (E)	**27.0 (E)**	19.1 (A)	22.6 (D)	20.6 (E)
Glydenlove2	0.9	12.0 (L)			**16.3 (A)**			13.7 (A)
Glydenlove1	1.0	13.1 (L)			13.1 (A)			12.3 (A)
Bernstorff	1.6	8.1 (L)			**13.1 (A)**			8.0 (A)
Skinfaxe	3.3		2.7 (L)	4.0 (L)	**7.7 (L)**	3.0 (L)	2.7 (L)	2.2 (L)
Guldfaxe	2.0		5.1 (L)	**6.3 (L)**	4.9 (L)	5.4 (L)	4.9 (L)	4.5 (L)
Heimdal	1.7	6.3 (L)		6.5 (L)	**11.0 (L)**	6.1 (L)	4.5 (L)	4.6 (L)
Mogens1	3.6	9.0 (L)		15.2 (L)	**N/A**	12.2 (L)	N/A	11.1 (L)
Mogens1	7.0	N/A		11.5 (L)	**12.2 (L)**	10.5 (L)	9.0 (L)	9.5 (L)

[a]Listed from north to south measured at distance stated along centerline profile from July or August 2008 front position (locations shown by black dots in Figure 2). Values are averages over distances of 300 m; bold values show fastest flow speed in time series. Data source: A, ASTER; L, Landsat 7; E, ENVISAT-ASAR; D, airborne lidar. N/A, no results available at that location on profile (in year when data are available; blank, no appropriate data available for that year). Sequences of speed for Helheim and Kangerdlugssuaq for speedup and subsequent slowdown on 2000–2001 to 2006 have been published [*Luckman et al.*, 2006; *Howat et al.*, 2007].

[b]Locations are in Figure 1.

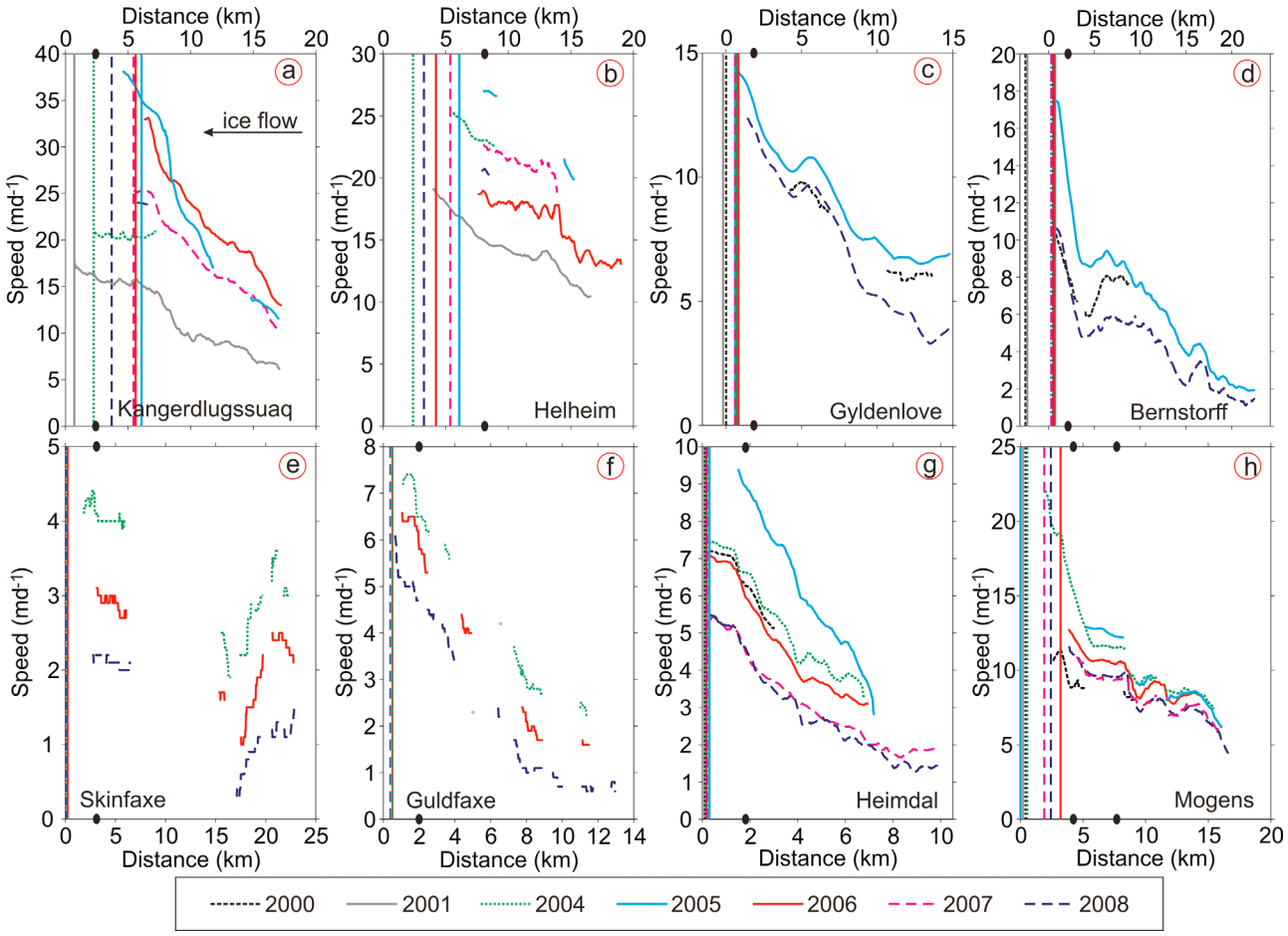

Figure 2. Summer speed profiles for sample of SE Greenland outlet glaciers (location in Figure 1) along central flow lines. Vertical lines show the July or August position of the glacier front in the year indicated. The 2008 speeds for Kangerdlugssuaq and Helheim were derived from ENVISAT-ASAR data and therefore show less coverage. Black dots on axes show location of speed data quoted in Table 2. Ice flow from right to left.

the averaging profile chosen or the location for which changes are quoted, the pattern described remains robust.

[17] Analysis of terminus positions showed that, in general, the glaciers retreated during the period to 2005 and then readvanced during the subsequent slowdown period (Figure 3). The slowdown, cessation of thinning and terminus stabilization was not just limited to the two outlet glaciers previously studied in detail, Helheim and Kangerdlugssuaq [*Howat et al.*, 2007; *Stearns and Hamilton*, 2007; *Joughin et al.*, 2008]: our results supplement those of *Howat et al.* [2008] and confirm that the entire SE Greenland region synchronously exhibited the same pattern of a significant slowdown and advance post-2005, which lasted until at least 2008.

4.2. Air Temperature, Runoff, and Accumulation

[18] Figure 4 shows the modeled runoff and accumulation for all the SE Greenland catchments throughout the time series, together with air temperature at Tasiilaq (location in Figure 1). In all catchments, both runoff and accumulation were highly variable through the 2000s (Figures 4b and 4c). Runoff was lowest during 2003 following the highest-accumulation winter in 2002–2003, and was particularly high in 2000, 2001, and 2006 following low-accumulation winters in 2000–2001 and 2005–2006.

[19] The relationship between air temperature and runoff is not straightforward. The air temperature record (Figure 4a) shows that winter 2002–2003 was anomalously warm in Tasiilaq and that the following summer was again warmer than normal for this period. Indeed during 2003 mean annual air temperature was positive for the first time since 1960 and was the highest since records began in 1895. Summer air temperatures in Tasiilaq remained high until 2005, before dropping slightly in 2006 and 2007. However, despite these higher coastal air temperatures, the mass balance model predicts that annual runoff production during 2003 was the lowest in these years throughout SE Greenland (Figures 4b and 4d). This low runoff follows high and prolonged snowfall in the previous winter in all catchments (Figures 4c and 4e), implying meltwater retention in the thicker snowpack. The model predicts that runoff increased after the 2003 minimum (Figure 4b), subsequently returning to normal, with the highest subsequent runoff thereafter predicted during 2006. This high runoff was caused by low snowfall during the preceding winter (Figure 4c and 4e). Thus, it is clear that both accumulation and runoff are highly variable and that there are

Table 3. Rate of Change of Surface Elevation for 24 Glacier Outlets Listed From North to South[a]

Glacier Name[b]	2004–2005	2005–2006	2006–2007	2007–2008
Kanger	−35	−4	−10	7
Kruuse	−9	−16	9	−5
Helheim	−34	12	11	8
Ikertivaq5	−23	−16	**−16**	−27
Ikertivaq4	−2	−8	**−8**	5
Ikertivaq3	3	−1	**−1**	−2
Ikertivaq2	6	5	**5**	−5
Ikertivaq1	−42	7	**7**	9
Koge4	N/A	−25	1	−8
Koge3	25	−27	−4	2
Koge2	−23	0	22	−21
Koge1	−7	−2	7	2
Gyldenlove2	N/A	2	−16	11
Gyldenlove1	N/A	−6	0	2
Bernstorff	N/A	3	3	−14
Skinfaxe	−6	15	15	−21
Guldfaxe	−5	31	−20	−20
Rimfaxe	−9	30	−16	−16
Heimdal	4	8	−8	3
Tingmiarmiut	N/A	N/A	10	−3
Mogens3	−12	−12	7	N/A
Mogens2	9	−8	−3	−8
Mogens1	−20	−11	1	7
Puistortuq	−30	−4	−2	−2
	2004–2005	2005–2006	2006–2007	2007–2008
Mean	−11.0	−1.1	−0.3	−4.2
Median	−9	−2	1	−3

[a]In meters per year. All from ASTER data, except Helheim data in 2007 and 2008 and Kangerdlugssuaq in 2007 from airborne lidar; other 2007 data from SPOT-5. N/A, no data available. Averaging profiles are 10 km long where data are available. Other profile lengths: Ikertivaq5, 9.4 km; Ikertivaq3, 7.3 km; Ikertivaq1, 5.4 km; Koge1, 8.3 km; Puistortuq, 9.9 km. Overall results are robust to changes in the chosen averaging length from the front margin (although quoted table values would change). Repeated bold values are based only on measurements at the beginning and end of the 2-year period shown and are therefore averaged across both years.
[b]Locations are in Figure 1.

regional trends across SE Greenland in both surface mass balance components. For the years we study, there seems to be a much stronger inverse relationship between the runoff in a year and the preceding year's snowfall than between runoff and summer temperatures.

[20] The south catchment (Figure 1) has the largest runoff and accumulation, with runoff removing the greatest percentage of accumulated snow. Even so, the model predicts that the mean percentage of accumulation melted as surface runoff is ~40% in the south catchment and is less than ~13% for all other catchments. This low value emphasizes that changes in mass loss from the front margin from iceberg calving and submarine melt will dominate the region's contribution to sea level rise.

4.3. Field Measurement of Ocean Temperatures

[21] At the measurement buoy location (Figure 1), salinity shows two annual peaks, in early spring and summer, which are clearest in the shallow records (Figure 5). The peaks are also present in the shallow temperature data, but unlike salinity, have different magnitudes. The early-spring peak is much smaller, coincides with a rise in salinity, and is normally followed by a drop in temperature and salinity in late spring and a summer temperature and salinity high. In this latter peak, temperature is usually higher than the early-spring event (Figures 5a and 5b). The late-spring freshening and cooling appears to be associated with the breakup and melt of sea ice, which presumably feeds cold freshwater into the ocean water (Figure 5c). Evidence for this comes additionally from the interannual relationship between sea ice and salinity, for example, in 2002 when low salinity followed high winter coastal sea ice and a strongly negative SSTA (Figure 5) and subsequently in 2003 when high salinity followed low winter sea ice coverage (discussed further below).

[22] The buoy data add evidence to the assertion that 2003 was an unusual year (Figures 5 and 6). Not only was the coastal air temperature unusually high (Figure 4a), clear temporal peaks in temperature and salinity occurred during 2003 (Figures 5a and 5b), with ocean temperatures reaching ~9°C at 20–50 m depth. Temperature versus salinity plots show that the summer waters were both unusually saline and warm (Figure 6), implying that Irminger Current waters dominated.

4.4. Sea Surface Temperature

[23] Figure 7 shows the regional SSTA from AVHRR data for June through September 2000–2008. These data show that coastal waters during this period were often colder than the baseline period. A negative SSTA developed in many years along the continental shelf through the summer with maximum definition in August–September. The AVHRR data also show the wide-scale nature of warmer water than the baseline period throughout summer 2003 (Figure 7). During summer 2004, there was a warm water anomaly north of Iceland, but colder water was present close to the SE Greenland coast, being especially apparent from Helheim southward (Figure 7), and colder water was also present at the coast southward of Kangerdlugssuaq Fjord during 2005. The strongest warm water anomaly of the time series between Iceland and Greenland occurred during July 2007; however, by September that year, a cold water anomaly was again present at the SE Greenland coast (Figure 5). Sea ice was observed along the coastline during June in most years but was largely absent by August in all years (Figure 8): during 2003, it was also absent in July.

[24] For 12 months from October 2002, the SSTA along the SE Greenland coast was positive (Figure 5e). From late spring 2005, the SSTA along the coast was negative for 24 months, showing that for 2 years the waters were colder than baseline. Indeed, except for a brief excursion to a positive anomaly during July and August 2007, coastal SSTA values have remained negative since 2005.

[25] There are many Landsat images covering the SE Greenland coast during our study period; hence, we present sequences of late August or September thermal images for the Kangerdlugssuaq and south catchments (Figures 1 and 9), which are the months when the AVHRR data (Figure 7) show the negative SSTA to be best developed.

[26] The Landsat SST data clearly show a cold water band at the SE Greenland coast that varied in width and temperature (Figure 9). Unfortunately no Kangerdlugssuaq image is available for 2003, but consistent with the AVHRR data images from this area, the Landsat data show the widespread occurrence of warm water at the coast during 2004 compared to other years (Figure 9a). In contrast, despite another warm water incursion during 2007, there was cold water at the coast

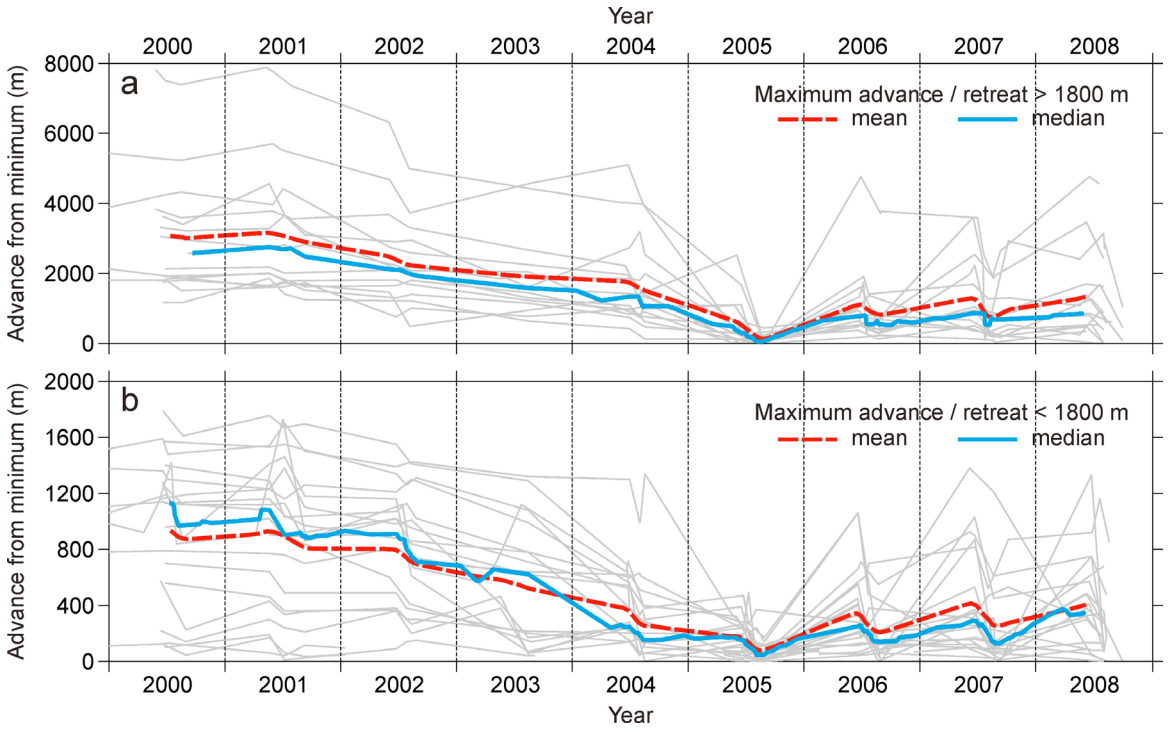

Figure 3. Calving front location of outlets separated on the basis of the range of advance/retreat exhibited: (a) those that retreat more and (b) less than 1800 m during 2000–2005. Trendlines are monthly running mean and median.

by early August southward of Kangerdlugssuaq. The southern images (Figure 9b) cover an area offshore from the south catchment and coincide with a region of narrow continental shelf (Figure 1). In this location there was a narrow band of cold water along the coast that varied in width from ~25 to 65 km between years.

5. Discussion

5.1. Observation of EGC/EGCC in SST Data

[27] In accordance with *Bacon et al.* [2002] we interpret the cold water band at the coast in Landsat data and the equivalent negative coastal SSTA in the AVHRR data as the expression of the EGC/EGCC (Figures 7 and 9). Using typical widths for the EGCC from the work of *Sutherland and Pickart* [2008], the SST of the EGCC was ~2°C lower than the EGC as measured from Landsat thermal data comparing average temperature between 3–33 km and 22–63 km from the coast [*Sutherland and Pickart*, 2008]. The Landsat data show the EGCC was narrowest and least well defined in 2003–2004; however, by late September 2005, a wide cold coastal surface water current was present (Figure 9). The SSTA in the AVHRR data concur with this interpretation.

[28] The Landsat images from the Kangerdlugssuaq catchment (Figure 9a) provide strong evidence for the EGCC starting at this location, in accordance with *Sutherland and Pickart* [2008], with little cold water transported along the coast from further north during this time of year. The images from 2000, 2005, and 2007 are the most supportive. However, our Landsat images do not support the suggestion that the EGCC forms due to the diversion of cold EGC waters through the Kangerdlugssuaq glacial trough (Figure 1) to the coast [*Sutherland and Pickart*, 2008]. Indeed, at Kangerdlugssuaq, the glacial trough appears to be delineated by high SSTs. While we must recognize that the SST is representative only of the very surface of the ocean, it is hard to explain the consistent high SSTs over the trough without warm water occurring at depth as well.

5.2. What Was the Cause of the Glacier Dynamic Event?

[29] The synchronous nature of the previously reported speedup and subsequent prolonged slowdown over such a large region rules out any local control, such as retreat of each glacier front into an overdeepening (as was suggested by *Howat et al.* [2008]). Thus, we examine two regional triggers for these responses. First, we consider air temperature and increased runoff, and second, the influence of ocean temperatures.

[30] Our mass balance modeling shows runoff in southeast Greenland was at a minimum in 2003 and low again in 2004, despite above average coastal air temperatures. The acceleration of these glaciers therefore occurs at a time of low runoff. Runoff was particularly high in 2006, which matches the period of maximum slowdown. On this basis, we reject increased surface runoff as the controlling factor for the increased speed of these SE Greenland tidewater glaciers, since their speedup is synchronous with reduced runoff, and their slowdown coincided with maximum runoff.

[31] Although the presence of a thick snowpack would limit catchment-wide runoff, higher coastal air temperatures would cause more melt close to the exposed glacier front. This increased melt would potentially increase water input and levels in crevasses and could drive increased circulation

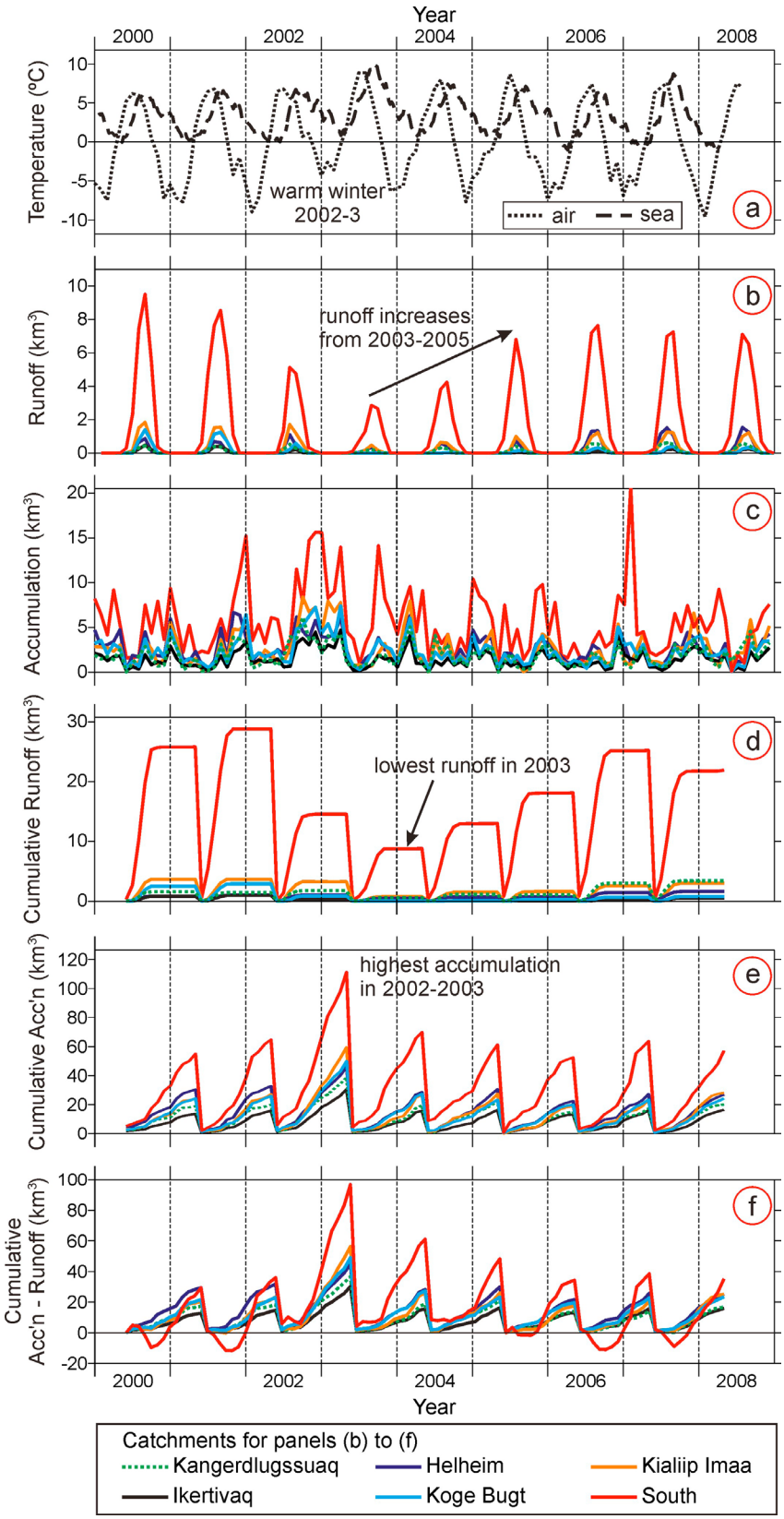

Figure 4. (a) Monthly air temperatures at Tasiilaq and sea surface temperature (SST) at the buoy location (from AVHRR SST product for August 2000–2008, http://iridl.ldeo.columbia.edu/SOURCES/.NOAA/.NCEP/.EMC/.CMB/.GLOBAL/.Reyn_SmithOIv2/.monthly/.sst/), (b and c) monthly runoff and accumulation, (d and e) cumulative yearly runoff and accumulation (May–April), and (f) cumulative accumulation-runoff (May–April) for each catchment in Figure 1.

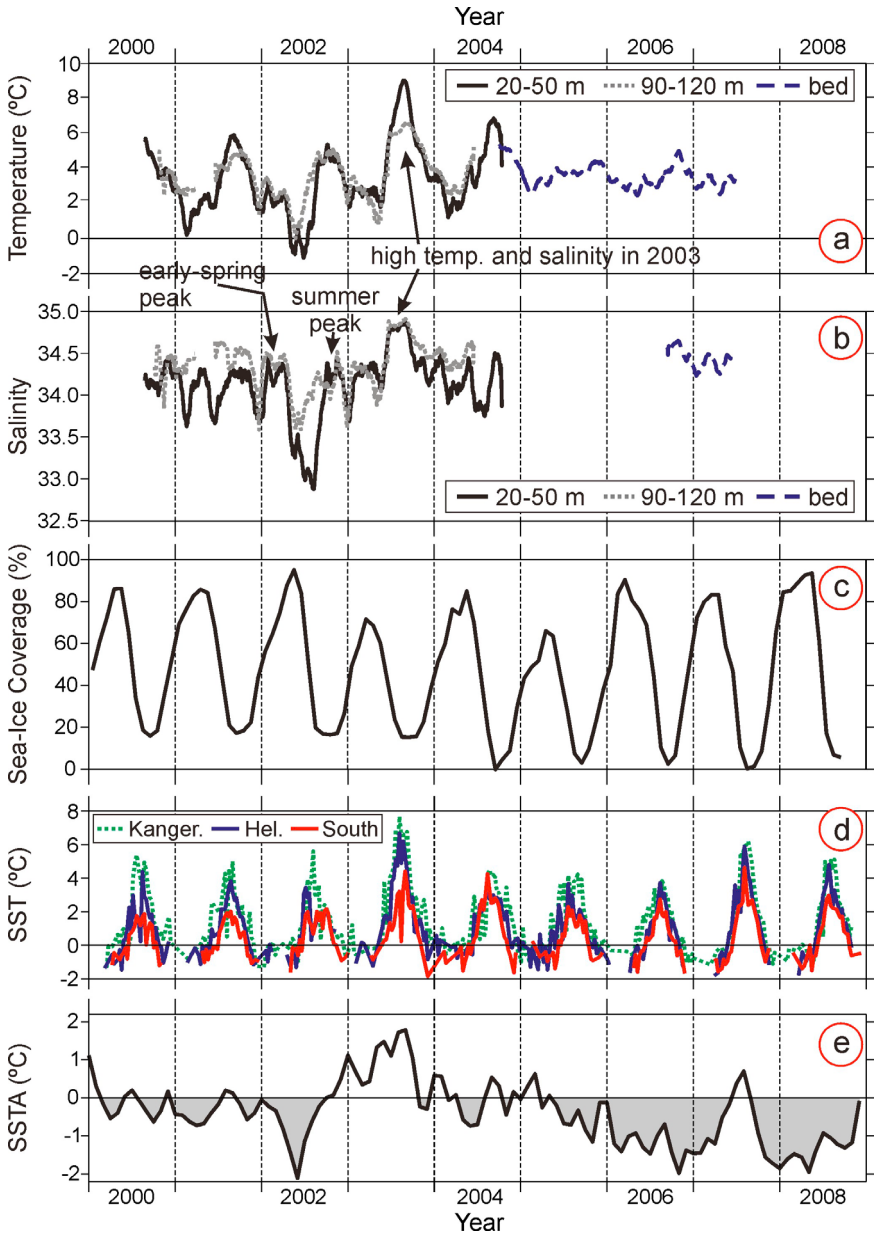

Figure 5. (a) Mooring temperature and (b) salinity mean daily data smoothed with a 29-point filter. Bed data were located at seabed at ~220 m depth. Salinity data are unitless (practical salinity units). (c) Mean monthly sea ice coverage (http://iridl.ldeo.columbia.edu/SOURCES/.NOAA/.NCDC/.OISST/.version1/.AVHRR/.ice/), averaged along a line ~1 km off the Greenland coast, between latitudes 61.5°N and 68.5°N. (d) Sea surface temperature at the mouth of fjords extracted from MODIS SST data, locations shown in Figure 1. (e) Monthly SSTA (http://iridl.ldeo.columbia.edu/SOURCES/.NOAA/.NCEP/.EMC/.CMB/.GLOBAL/.Reyn_SmithOIv2/.monthly/.ssta/) along same line as Figure 5c. Note that the SSTA is relative to a 1971–2000 baseline.

at the calving front, both of which can increase iceberg calving rates [*Benn et al.*, 2007; *Motyka et al.*, 2003]. Coastal air temperatures at Tasiilaq were higher than usual during 2003–2005 (Figure 4a), whereas on 2006 and 2007 they were lower (albeit higher than 2000–2002). The minor reactivation at Helheim in 2007 occurred when air temperatures were not significantly higher than the preceding year (Figure 4a). Thus, there is no strong correlation between air temperature and the glacier dynamic changes we report. However, it should be noted that Tasiilaq is located close only to Helheim and Ikertivaq glaciers, and so, without further evidence, this effect cannot be wholly ruled out as the driver for these dynamic changes. Furthermore, coastal air temperatures and SST are clearly interrelated.

[32] The other regional factor linking the outlet glaciers in SE Greenland is the ocean [cf. *D. M. Holland et al.*, 2008; *Straneo et al.*, 2010]. Although the mooring data show water conditions only at a single point, the warm saline water recorded at depth in 2003 was clearly part of a widespread anomaly on the SE Greenland coast that year as evident in the

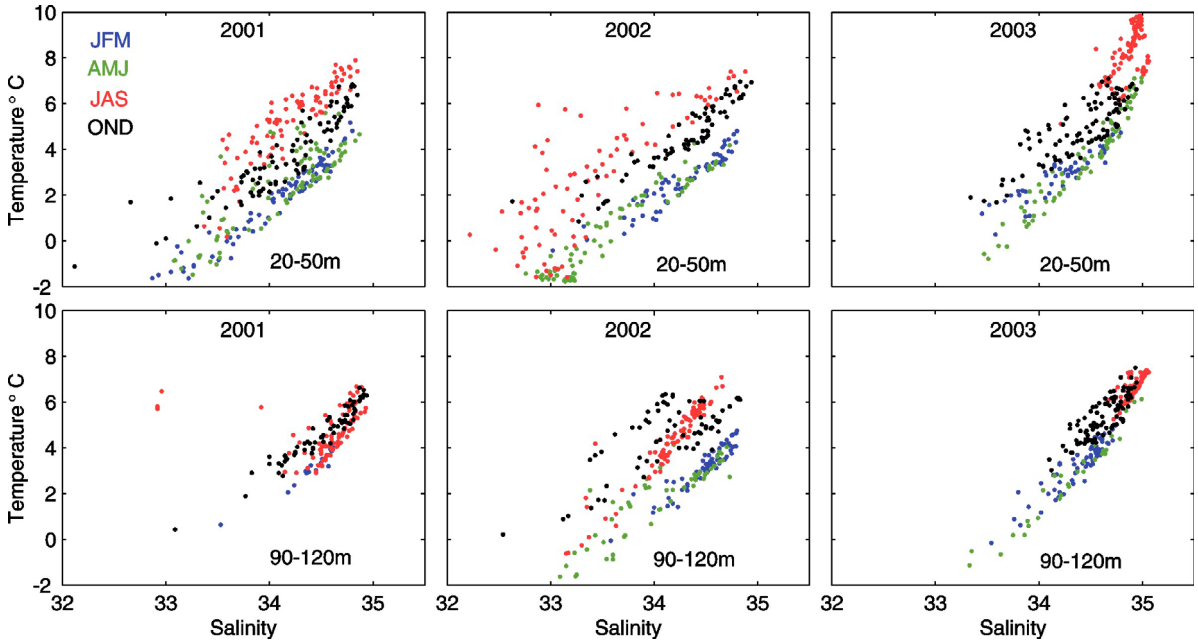

Figure 6. Daily mean temperature versus salinity plots at (top) 20–50 m and (bottom) 90–120 m colored by season for the years 2001, 2002, and 2003. The Irminger Current waters are clearly dominant in summer months of 2003 at both depths, showing virtually no mixing with fresher coastal current waters of the EGC or EGCC.

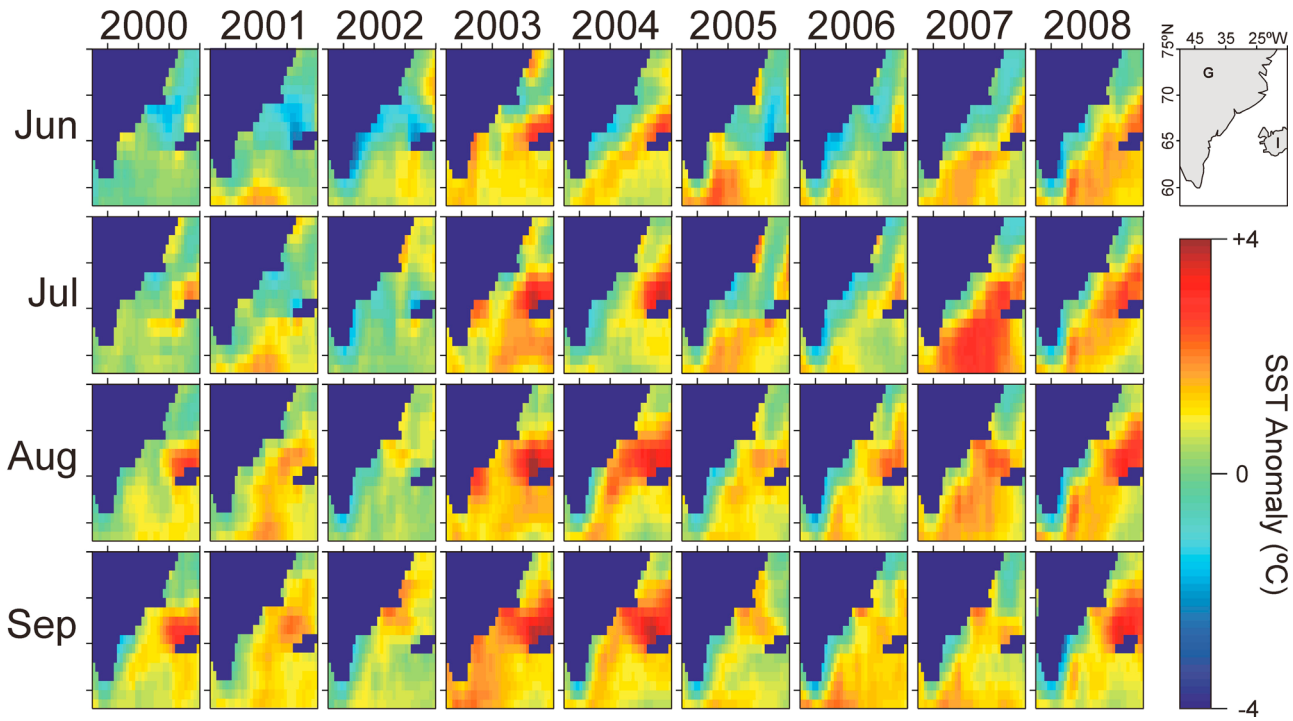

Figure 7. SSTA June–September for 2000–2008 from Optimal Interpolation product (http://iridl.ldeo.columbia.edu/SOURCES/.NOAA/.NCEP/.EMC/.CMB/.GLOBAL/.Reyn_SmithOIv2/.monthly/.ssta/). Inset shows the area of maps: G, Greenland; I, Iceland. Note that the SSTA is relative to a 1971–2000 baseline.

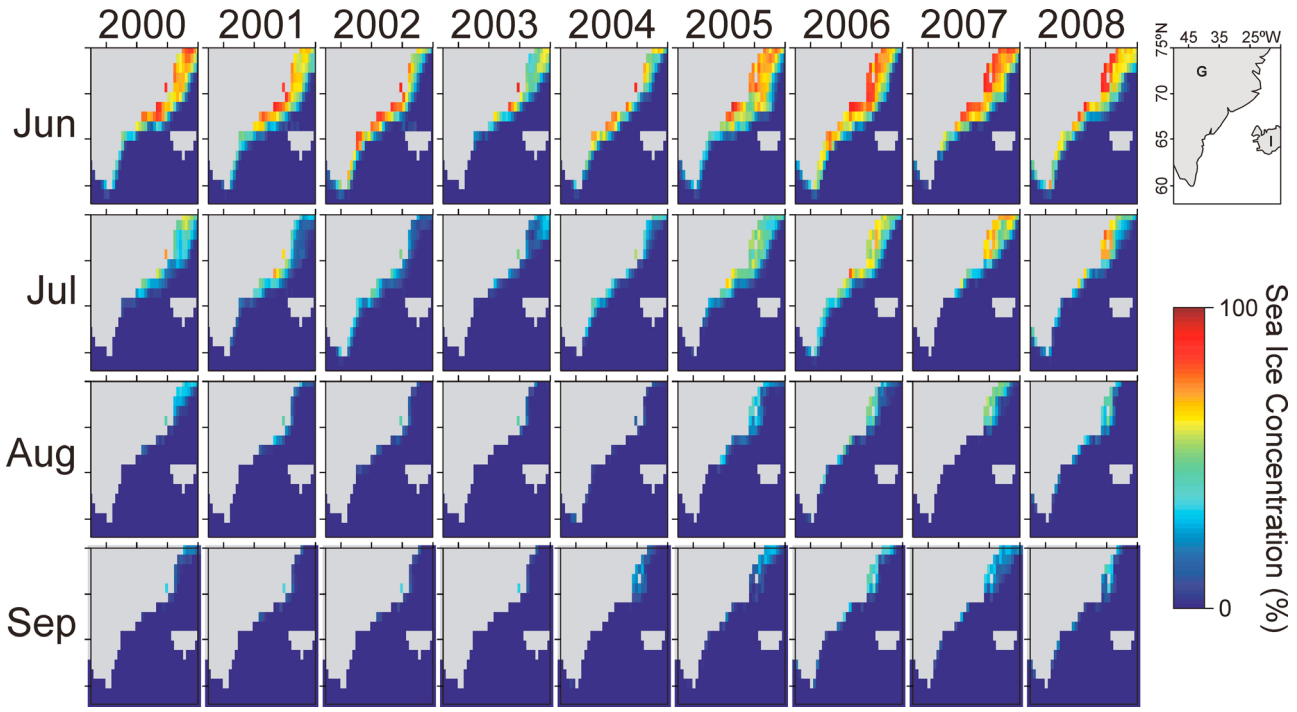

Figure 8. Sea ice concentration June–September for 2000–2008 from AVHRR sea ice product. Inset shows the area maps: G, Greenland; I, Iceland.

satellite data: (1) SSTA and SST data show warmer coastal waters than normal, with warm water at the coast by late summer 2003 (August and September; Figures 7 and 9); (2) there was a high-salinity cap on the shelf waters at Kap Farvel (location in Figure 1) during 2003, compared to 2001, 2002, or 2004 [*Sutherland and Pickart*, 2002]; and (3) warm waters of Irminger Current origin were present at depth in Kangerdlugssuaq fjord during 2004 [*Christoffersen et al.*, 2008], when there was a positive SSTA at the coast north of Ikertivaq (Figure 7).

[33] Thus, following high air temperatures in winter 2002–2003, summer 2003 had anomalously high ocean and fjord water temperatures (Figures 5a, 7, and 9). We propose that this warm water reduced fjord ice and the presence of the mélange during winters 2003–2004 and 2004–2005. For example, Landsat imagery (row 14, path 231) shows water in Sermilik Fjord close to Helheim glacier's front in mid-April/early-May 2004 and 2005, whereas in 2003 the mélange was solid at this time, and in 2006 there was extensive fjord ice. We postulate that as a consequence of the warm waters and minimal fjord ice, the speed and calving rate of the glaciers increased, with fastest flow and highest calving rates during 2004 or 2005. During 2004 and 2005, a negative SSTA can be seen at the coast in late summer, albeit weak in 2004 (Figures 5 and 7). This SSTA was well established in summer 2005 (Figures 5 and 7), and cold surface water hugged the coast, marking an apparent recovery of the EGCC. Water temperatures along the coast continued to drop through 2006 (Figure 5e) synchronous with a slowdown of the glaciers. High ocean temperatures occurred offshore in 2007; however, the presence of cold coastal waters (Figure 7) meant there was only minor glacier reactivation.

[34] Our interpretation of these data is that the dynamics of these glaciers are controlled principally by the temperature of the ocean waters. It is clear that in order for this to occur there must be exchange of waters between the coast and the fjords, with the warm water at the coast entering the fjords and reaching the glacier front margins. This exchange appears to occur on both the west coast of Greenland, with warm water impacting the velocity of Jakobshavn Isbrae [*D. M. Holland et al.*, 2008], and the east coast, where warm waters have been reported in both Kangerdlugssuaq [*Christoffersen et al.*, 2008] and Sermilik [*Straneo et al.*, 2010] fjords. Warm surface water is clearly visible in the Landsat SST at the location of major troughs (e.g., compare Figure 1 and Figure 9), including Helheim and Kangerdlugssuaq, suggesting that warm water is routed toward the coast via these bathymetric features. At Jakobshavn, the arrival of warm water in the fjord required it to overtop the shallow sill at the fjord mouth [*D. M. Holland et al.*, 2008]. While the bathymetry of all of the SE Greenland fjords is not well known, neither Sermilik nor Kangerdlugssuaq fjords have coastal sills [*Buch*, 2002], so there should be little impediment to the exchange of water between the fjords and the ocean. However, we note that the processes of water circulation within these fjords, their bathymetry, and the subsequent impact of this water on the glacier front and glacier dynamics are poorly constrained and require further research. Undercutting of the calving cliff, melt beneath any floating tongue or mélange, and changes in circulation at the glacier front [*Motyka et al.*, 2003] are likely to be key controls.

5.3. Do the Glaciers Affect the EGCC?

[35] Having shown a possible connection between coastal waters and glacier dynamics in SE Greenland, we next consider the contribution of these glaciers to the cold freshwaters of the EGCC. It is clear that the 2003–2005 speedup resulted in large volumes of icebergs being calved from these glaciers,

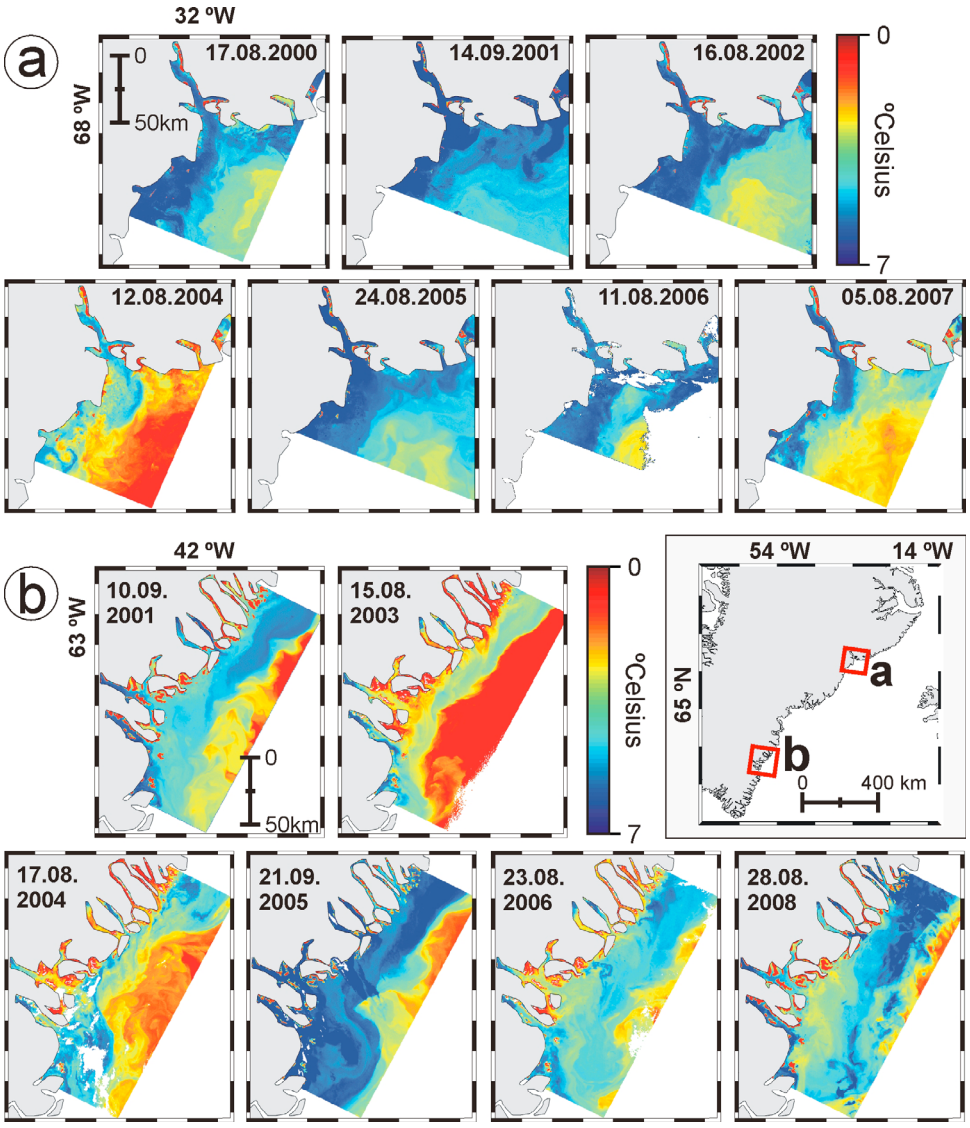

Figure 9. Late August–September Landsat thermal images calibrated as described in text. Most clouds and land are masked so that images show sea surface temperature, but occasional cloud contamination remains. Red box shows extent of satellite scene coverage. Note that there is no cloud-free image for this period during 2003 or 2008 in the northern area and none in 2002 or 2007 in the southern.

most of which will have melted in the fjords or in transport along the coast, thus directly contributing to the coastal EGCC. Unfortunately, there are no ice thickness estimates for most of the glacier catchments, making a robust estimate of the iceberg input to the EGCC difficult. *Rignot and Kanagaratnam* [2006] estimated the iceberg output from this region as ~220 km^3 at the height of the dynamic event in 2005, an increase of ~70 km^3 discharge over that of 2000. Helheim, where glacier thickness is known from airborne lidar and ice-penetrating radar sensors operated by NASA and the University of Kansas, respectively, discharged ~50 km^3 as icebergs or ice cliff melt during 2005, which was an increase of ~61% over its discharge in 2000. These figures suggest an estimate of around 130–180 km^3 of icebergs calved into the coastal waters from the SE Greenland catchments during 2000 and 200–250 km^3 during 2005.

[36] In addition to the iceberg contribution to the current, we must also consider meltwater runoff from the glaciers and from snowmelted in unglaciated parts of the fjord catchments together with changes in these contributions over time. Although runoff produces less water volume than iceberg calving (Figure 3 and Table 1), the water is produced at the glacier front or runs directly into the fjord and may hence have more impact on the glacier than icebergs that melt within the coastal current. As noted above, the lowest glacial runoff in the time series was recorded in 2003 (~10.5 km^3). After a small increase in 2004 (Figure 3b), runoff in 2005 was almost back to the normal for this period (~22 km^3). By 2006 and 2007, annual runoff from the glaciers was ~30 km^3.

[37] 2004 and 2005 were years of both increasing iceberg calving and increasing ice sheet runoff. Together iceberg melt and runoff must have contributed significant additional cold

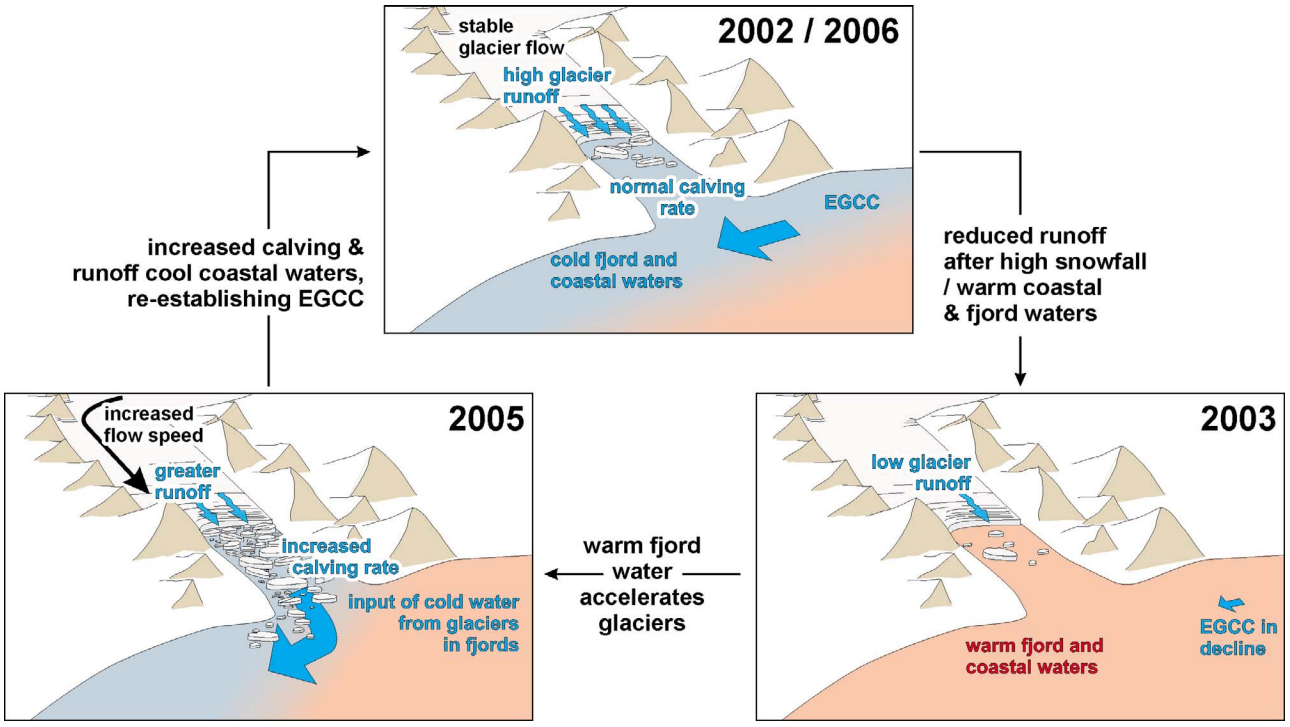

Figure 10. Schematic showing the hypothesized negative feedback from increased iceberg discharge and runoff when the SE Greenland outlet glaciers accelerate or lose additional mass through increased surface melting.

freshwater to the coastal waters of the EGCC during those years. The volume contribution during summer 2005 from the whole SE Greenland coast was around 220–270 km^3, with the availability of this freshwater increasing southward along the coast. We hypothesize that this ice sheet–derived water (icebergs plus meltwater) is the cause of the negative coastal SSTA developed during the later summer months. This cold water is clearly observed in the Landsat SST images, in which Kangerdlugssuaq is seen contributing a plume of cold water into the coastal waters (Figure 9). We further suggest that this water makes a significant contribution to the EGCC, at least later in the summer [cf. *Bacon et al.*, 2002].

[38] Is the volume of water and ice added by iceberg calving and glacier runoff sufficient to affect the temperature of the EGCC? If we assume the discharge from the ice sheet calculated above occurs evenly distributed over a 100 day period in summer, then we can compare this flux with the total transport in the EGCC, ~0.8 Sv [*Bacon et al.*, 2002]. This simple calculation suggests ~3%–4% of total volume of the waters in the EGCC results from iceberg calving and ice sheet runoff. Assuming the ice sheet–derived water is at 0°C and 0 salinity, this flux would reduce the temperature of the EGCC by 0.2°C–0.25°C and salinity by 1–1.4 for the whole of this period. However, much of the discharge is icebergs, which take up a latent heat flux when they melt, cooling their surroundings. Icebergs take about 12–24 days to travel along the coast in the EGCC if it is flowing at 0.5–1.0 m s^{-1} [*Sutherland and Pickart*, 2008]. Each km^3 of ice at 0°C that melts has the potential to lower a water mass of the volume of the EGCC by ~0.05°C. If ~50% of the ice melts in transit and ~1/5 of the icebergs calved are in transit at any time in the 100 days of summer then the minimum estimate for 2005 of the melting of 50% of 200 km^3 of ice will lower the temperature of the EGCC by ~1°C over the 100 days.

[39] This calculation is clearly simplistic, ignoring, for example, the likelihood of icebergs being at temperatures below 0°C and the storage of icebergs within the ice mélange. However, it does show the potential for the temperature and salinity of the EGCC to be seasonally and interannually affected by the discharge from these glaciers.

[40] It seems that ice sheet runoff and iceberg melt can make a significant contribution to the temperature and salinity of the EGCC during summer. The interpretation is further supported by (1) the difference between air and sea surface temperature being greatest in 2005 when iceberg calving rates were highest (Figure 4a); (2) comparison of mooring and SSTA data: lowest temperatures at the former typically occur in late spring (around May) due presumably to sea ice breakup (Figure 5a); subsequent negative SSTA in the EGCC values during August (Figure 7) must be due to runoff and calving; and (3) the coastal positive SSTA started to reduce in 2005 (Figure 5e), which must therefore have resulted from ice sheet sources because there was low coastal sea ice coverage that year (Figure 5c).

5.4. Feedback Between Glaciers and the EGCC

[41] We propose that the glaciers themselves contributed to their own slowdown in a negative feedback with the waters of the EGCC (Figure 10). Faster flow was initiated when coastal waters were warm, resulting from a weak EGCC at a time of low meltwater runoff and calving. The glaciers sped up, increasing their calving rates while runoff also recovered. This increased ice discharge from the ice sheet delivered additional cold water into the EGCC, contributing to its

recovery and acting to stabilize the flow speeds of SE Greenland glaciers. Thus, we suggest that the ice sheet's input to the EGCC provides a negative feedback, which tends to restabilize these sensitive SE Greenland glaciers if their ice discharge increases substantially (Figure 10). However, we also note that there has been an overall increase in temperatures within North Atlantic waters [e.g., *Todd et al.*, 2008] and the Irminger Current [*Myers et al.*, 2007] in recent decades, which might drive a regional trend, or more frequent or larger glacier dynamic events, in response to warm water incursions.

6. Conclusions

[42] The early 2000s speedup of SE Greenland tidewater outlet glaciers was followed by a widespread and synchronous slowdown event, which suggests that the first-order dynamic control is regional. Runoff lubrication of the glaciers does not provide the explanation for this speedup/slowdown event, and there is evidence that increased surface melt at the front is also not the dominant control. We suggest that the speedup was the result of warm ocean waters coming into contact with the glaciers and have identified an important control on the glaciers' response, namely the cold waters of the coastal EGCC, which weakened during the speedup and restrengthened coincident with the slowdown. We have also suggested a negative feedback that currently mitigates against continued very fast loss of ice from the ice sheet in a warming climate.

[43] Our results suggest that regional ocean forcings play an important part in controlling the dynamics of the SE Greenland glaciers. Since these SE Greenland outlet glaciers have dominated recent changes in ice sheet mass loss, the negative feedback we identify will also help regulate Greenland's contribution to sea level rise against a background of increasing ocean temperatures. We should expect similar speedup and slowdown events of these glaciers in the future, which will make it difficult to elucidate any underlying trend in mass loss resulting from changes in this sector of the ice sheet.

[44] Finally, we recognize that the water in the glacier fjords on the SE Greenland coast will act as an important buffer between warm ocean water and the glaciers themselves. We do not believe that current knowledge about water circulation in these fjords is sufficient, nor about the processes that would control the impacts and time scales of water reaching the ice or the duration of its impact. We thus suggest the processes of fjord water circulation and its effect on glacier dynamics as high priorities for future research.

[45] **Acknowledgments.** The *GLIMPSE* project is funded through the Leverhulme Trust Research Leadership Scheme. T.D.J. was in part funded by the European Union through the Welsh Assembly Government, and S.R.D. was funded through Defra-SD0440, Damocles (financed by the EU in 6th Framework Programme for R&D) with support of ASOF-EU and WHOI-OCCI. The moorings were deployed by University of Hamburg and Cefas, with thanks to ships' crew, chief scientists, and technicians. We thank the European Space Agency, the SPIRIT Initiative, and NASA for the award of Envisat, SPOT-5, and ASTER data, respectively; ECMWF for reanalysis (ERA-40) and operational analysis data; and Danish Meteorological Institute for Tasiilaq air-temperature data. The NERC ARSF collected airborne lidar in 2007 and the Cryospheric Sciences Branch of NASA Goddard Space Flight Center in 2008. S. Bevan created the drainage basin outlines, and M. Duijkers produced the MODIS temperature profiles. The authors are grateful to the reviewers and associate editor who helped to improve the paper.

References

Amundson, J. M., M. Fahnestock, M. Truffer, J. Brown, M. P. Luthi, and R. J. Motyka (2010), Ice melange dynamics and implications for terminus stability, Jakobshavn Isbrae, Greenland, *J. Geophys. Res.*, *115*, F01005, doi:10.1029/2009JF001405.

Armstrong, E. (2002), MODIS Sea Surface Temperature (SST) Products, *Rep. CL 02-0691*, Jet Propul. Lab., Pasadena, Calif. (Available from http://podaac.jpl.nasa.gov/pub/documents/dataset_docs/modis_sst.html.)

Bacon, S., G. Reverdin, I. G. Rigor, and H. M. Snaith (2002), A freshwater jet on the East Greenland shelf, *J. Geophys. Res.*, *107*(C7), 3068, doi:10.1029/2001JC000935.

Bamber, J. L., S. Ekholm, and W. B. Krabill (2001), A new, high-resolution digital elevation model of Greenland fully validated with airborne laser altimeter data, *J. Geophys. Res.*, *106*(B4), 6733–6745, doi:10.1029/2000JB900365.

Benn, D. I., N. R. J. Hulton, and R. H. Mottram (2007), "Calving laws", "sliding laws" and the stability of tidewater glaciers, *Ann. Glaciol.*, *46*, 123–130.

Buch, E. (2002), Present oceanographic conditions in Greenland waters, 39 pp., *Sci. Rep. 02-02*, Danish Meteorol. Inst., Copenhagen.

Cappelen, J., E. V. Laursen, P. V. Jørgensen, and C. Kern-Hansen (2008), DMI monthly climate data collection 1768–2007, Denmark, The Faroe Islands and Greenland, *Tech. Rep. 08-4*, Danish Meteorol. Inst., Copenhagen. (Available from www.dmi.dk/dmi/index/viden/dmi-publikationer/tekniskerapporter.htm.)

Christoffersen, P., K. J. Heywood, J. A. Dowdeswell, J. P. Syvitski, T. J. Benham, R. I. Mugford, I. Joughin, and A. Luckman (2008), Warm Atlantic water drives Greenland Ice Sheet discharge dynamics, *Eos Trans. AGU*, *89*(53), Fall Meet. Suppl., Abstract C31B-0501.

Ekholm, S. (1996), A full coverage, high-resolution, topographic model of Greenland computed from a variety of digital elevation data, *J. Geophys. Res.*, *101*, 21,961–21,972, doi:10.1029/96JB01912.

Hanna, E., P. Huybrechts, I. Janssens, J. Cappelen, K. Steffen, and A. Stephens (2005), Runoff and mass balance of the Greenland ice sheet: 1958–2003, *J. Geophys. Res.*, *110*, D13108, doi:10.1029/2004JD005641.

Hanna, E., J. McConnell, S. Das, J. Cappelen, and A. Stephens (2006), Observed and modeled Greenland ice sheet snow accumulation, 1958–2003, and links with regional climate forcing, *J. Clim.*, *19*, 344–358.

Holland, D. M., R. H. Thomas, M. H. Ribergaard, and B. Lyberth (2008), Acceleration of Jakobshavn Isbræ triggered by warm subsurface ocean waters, *Nat. Geosci.*, *1*, 659–664, doi:10.1038/ngeo316.

Holland, P. R., A. Jenkins, and D. M. Holland (2008), The response of ice shelf basal melting to variations in ocean temperature, *J. Clim.*, *21*, 2558–2572, doi:10.1175/2007JCLI1909.1.

Howat, I. M., I. R. Joughin, and T. A. Scambos (2007), Rapid changes in ice discharge from Greenland outlet glaciers, *Science*, *315*, 1559–1561.

Howat, I. M., I. Joughin, M. Fahnestock, B. E. Smith, and T. A. Scambos (2008), Synchronous retreat and acceleration of southeast Greenland outlet glaciers 2000–2006: Ice dynamics and coupling to climate, *J. Glaciol.*, *54*, 646–660.

Jakobsson, M., R. Macnab, M. Mayer, R. Anderson, M. Edwards, J. Hatzky, H.-W. Schenke, and P. Johnson (2008), An improved bathymetric portrayal of the Arctic Ocean: Implications for ocean modeling and geological, geophysical and oceanographic analyses, *Geophys. Res. Lett.*, *35*, L07602, doi:10.1029/2008GL033520.

Joughin, I., I. Howat, R. B. Alley, G. Ekstrom, M. Fahnestock, T. Moon, M. Nettles, M. Truffer, and V. C. Tsai (2008), Ice-front variation and tidewater behavior on Helheim and Kangerdlugssuaq glaciers, Greenland, *J. Geophys. Res.*, *113*, F01004, doi:10.1029/2007JF000837.

Luckman, A., T. Murray, R. de Lange, and E. Hanna (2006), Rapid and synchronous ice-dynamic changes in East Greenland, *Geophys. Res. Lett.*, *33*, L03503, doi:10.1029/2005GL025428.

Luthcke, S. B., H. J. Zwally, W. Abdalati, D. D. Rowlands, R. D. Ray, R. S. Nerem, F. G. Lemoine, J. J. McCarthy, and D. S. Chinn (2006), Recent Greenland ice mass loss by drainage system from satellite gravity observations, *Science*, *314*, 1286–1289.

Moon, T., and I. Joughin (2008), Changes in ice front position on Greenland's outlet glaciers from 1992 to 2007, *J. Geophys. Res.*, *113*, F02022, doi:10.1029/2007JF000927.

Motyka, R. J., L. Hunter, K. A. Echelmeyer, and C. Connor (2003), Submarine melting at the terminus of a temperate tidewater glacier, LeConte Glacier, Alaska, U.S.A., *Ann. Glaciol.*, *36*(1), 57–65.

Myers, P. G., N. Kulan, and M. H. Ribergaard (2007), Irminger Water variability in the West Greenland Current, *Geophys. Res. Lett.*, *34*, L17601, doi:10.1029/2007GL030419.

Nick, F. M., A. Vieli, I. M. Howat, and I. Joughin (2009), Large-scale changes in Greenland outlet glacier dynamics triggered at the terminus, *Nat. Geosci.*, *2*, 110–114, doi:10.1038/ngeo394.

Pfeffer, W. T. (2007), A simple mechanism for irreversible tidewater glacier retreat, *J. Geophys. Res.*, *112*, F03S25, doi:10.1029/2006JF000590.

Reynolds, R. W., N. A. Rayner, T. M. Smith, D. C. Stokes, and W. Wang (2002), An improved in situ and satellite SST analysis for climate, *J. Clim.*, *15*(13), 1609–1625.

Rignot, E., and P. Kanagaratnam (2006), Changes in the velocity structure of the Greenland Ice Sheet, *Science*, *311*, 986–990.

Sandven, S., K. Kloster, and K. F. Dagestad (2007), Ice drift in the Fram Strait from Envisat ASAR data, paper presented at Envisat Symposium 2007, Montreux, Switzerland.

Scambos, T. A., M. J. Dutkiewicz, J. C. Wilson, and R. A. Bindschadler (1992), Application of image cross-correlation to the measurement of glacier velocity using satellite image data, *Remote Sens. Environ.*, *42*, 177–186.

Stearns, L. A., and G. S. Hamilton (2007), Rapid volume loss from two East Greenland outlet glaciers quantified using repeat stereo satellite imagery, *Geophys. Res. Lett.*, *34*, L05503, doi:10.1029/2006GL028982.

Straneo, F., G. S. Hamilton, D. A. Sutherland, L. A. Stearns, F. Davidson, M. O. Hammill, G. B. Stenson, and A. Rosing-Asvid (2010), Rapid circulation of warm subtropical waters in a major glacial fjord in East Greenland, *Nat. Geosci.*, *3*, 182–186, doi:10.1038/NGEO764.

Strozzi, T., A. Luckman, T. Murray, U. Wegmüller, and C. Werner (2002), Glacier motion estimated using SAR offset-tracking procedures, *IEEE Trans. Geosci. Rem. Sens.*, *40*(11), 2384–2391.

Sutherland, D. A., and R. S. Pickart (2008), The East Greenland Coastal Current: Structure, variability, and forcing, *Prog. Oceanogr.*, *78*, 58–77.

Sutherland, D. A., R. S. Pickart, E. P. Jones, K. Azetsu-Scott, A. J. Eert, and J. Ólafsson (2009), Freshwater composition of the waters off southeast Greenland and their link to the Arctic Ocean, *J. Geophys. Res.*, *114*, C05020, doi:10.1029/2008JC004808.

Todd, C. D., S. L. Hughes, C. T. Marshall, J. C. MacLean, M. E. Lonergan, and E. M. Biuw (2008), Detrimental effects of recent ocean surface warming on growth condition of Atlantic salmon, *Glob. Ch. Biol.*, *14*, 958–970, doi:10.1111/j.1365-2486.2007.01522.x.

Wouters, B., D. Chambers, and E. J. O. Schrama (2008), GRACE observes small-scale mass loss in Greenland, *Geophys. Res. Lett.*, *35*, L20501, doi:10.1029/2008GL034816.

Zwally, H. J., W. Abdalati, T. Herring, K. Larson, J. Saba, and K. Steffen (2002), Surface melt-induced acceleration of Greenland ice sheet flow, *Science*, *297*(5579), 218–222, doi:10.1126/science.1072708.

A. D. Booth, S. Cook, A. L. C. Hughes, T. D. James, A. Luckman, T. Murray, K. Scharrer, and N. Selmes, GLIMPSE Research Group, Department of Geography, Swansea University, Swansea SA2 8PP, UK. (t.murray@swansea.ac.uk)

S. R. Dye, Centre for Environment Fisheries and Aquaculture Science, Lowestoft Laboratory, Pakefield Rd., Lowestoft NR33 0HT, UK.

E. Hanna, Department of Geography, University of Sheffield, Winter St., Sheffield S10 2TN, UK.

P. Huybrechts, Department of Geography, Vrije Universiteit Brussel, Pleinlaan 2, B-1050 Brussels, Belgium.